10
Microfluidic Systems for Whole-Animal Screening with *C. elegans*

Navid Ghorashian, Sertan Kutal Gökçe, and Adela Ben-Yakar

10.1
Importance

We discuss emerging microfluidic technologies that enable new capabilities in whole-animal studies on *Caenorhabditis elegans*. This nematode is one of the most well-characterized *in vivo* models in molecular biology and has been used to produce significant findings related to all areas of biology, especially neurological function, behavior, and disease. Microfluidic devices can easily manipulate these organisms in a high-throughput fashion to perform automated studies on a large scale using high-resolution optical interrogation and imaging methods. This chapter focuses on the applications using *C. elegans* to enhance the understanding and treatment of neurodegenerative disease.

10.2
Introduction

Within molecular biology, a vast array of technologies has enabled faster and more comprehensive characterizations of the fundamental biology related to human disease. For example, the potential impact of understanding these mechanisms in relation to neuron regeneration and degeneration would have profound benefits for those suffering from severe disorders of the nervous system (e.g., Alzheimer's, Parkinson's, and Huntington's diseases), as well as injuries (e.g., acute trauma, spinal cord damage). These conditions are some of the most devastating ailments known to modern medicine [1, 2]. A major step toward enhancing fundamental knowledge of such diseases would be to elucidate their molecular pathways in well-understood *in vivo* systems that can be comprehensively characterized [3–6].

One such model organism is the roundworm *C. elegans.* The worm's amenability to a plethora of molecular tools, nearly complete genetic and morphological characterization, and simple cultivation requirements have led to unprecedentedly fast and comprehensive studies that were impractical with other *in vivo*

Micro- and Nanosystems for Biotechnology, First Edition. Edited by J. Christopher Love.

models [4, 7–9]. Fast generation times (3 days between larval and adult stages) and simplified genetics allow the creation of mutant strains in a matter of weeks, instead of months or years, which is typical for more complex model organisms. In fact, since its adoption by the molecular biology community, research labs centered on this worm as their main research tool have emerged all over the world. The aforementioned benefits of using *C. elegans* as a model organism have allowed the yearly publication rate of worm-related papers to double from 2000 to 2010 [10]. Still, conventional experimental approaches have limited the size and speed of these studies. New technologies must be developed to automate and accelerate data collection, while maintaining information resolution in order to preserve the full benefits of *C. elegans* or similar experimental models.

With the considerable time and resources needed for comprehensive biological studies, such as genome-wide screens, recent studies have turned to microtechnology to create automated tools for the manipulation of microscopic biological samples with unprecedented speed and precision, as well as enhanced data output and analysis. Specifically, the application of microfluidic engineering has yielded an array of new high-throughput biological platforms [11–15]. Advances in microfabrication techniques vastly improved the speed, flexibility, and applicability of electronic devices by reducing the size and cost of complex electronic circuits. Microfluidics exploits these methods to make systems of microchannels that reduce the scale, cost, and processing time of manipulating chemical and biological samples. Moving toward the realization of large-scale integrated microfluidic platforms, several research groups have implemented microfluidic devices consisting of intricate arrays of pressure-controlled valves for multiplex chemical and visual analysis of biological samples [12–18]. These approaches have been applied and expanded upon to develop microfluidic platforms for the manipulation and interrogation of *C. elegans* worms for a variety of novel studies in neurobiology, while enabling the animals' use in next generation, high-throughput screens.

10.3 A Versatile Animal Model: *Caenorhabditis elegans* (*C. elegans*)

C. elegans is a nematode worm used across the biological sciences as a practical animal model for a variety of areas of biology, such as development, metabolism, and neuroscience. In the 1960s, Nobel Prize–winning scientist, Sydney Brenner identified *C. elegans* as an ideal model for molecular biology [19]. Though it is a simple multicellular organism (959 total cells, 302 neurons) that can be comprehensively understood at the morphological and genetic level, *C. elegans* retains sufficient genetic homology with mammals within its cellular and molecular machinery such that it can be used to study human disease. Simple genetics and culturing conditions make it one of the easiest *in vivo* tools to analyze and adopt into various experimental applications.

10.3.1 *C. elegans* Culturing Techniques

The simplicity of cultivating and maintaining *C. elegans* is a key advantage in using it to advance research in fundamental biomolecular phenomena. These animals can be grown in nonsterile environments without the need for stringent control of gas composition or humidity [20, 21]. While tighter control of these environmental parameters will tune animal viability, growth, behavior, and experimental outcomes to a finer degree, for many studies it is sufficient to cultivate the animals at room temperature on the lab bench. Typically, researchers raise *C. elegans* on agar plates seeded with *E. coli* bacteria (*Escherichia coli*, OP50 or HB101 strain) along with various salts and fatty acids for nutrition.

For liquid-based assays, *C. elegans* can be easily grown in liquid culture with bacteria (S medium) [21]. Such suspensions have several advantages over the essentially flat culturing substrates on agar pads in terms of simplicity, cost, and compatibility for large-scale studies. This approach is simpler and more cost effective because the liquid flask can easily accommodate a large volume of worms and bacterial food, which can be replaced by simply adding a fresh supply to the flask instead of regularly transferring the worms to brand new plates via resuspension and centrifugation. In liquid culture, worms receive much more uniform exposure to drugs across the entire population in comparison to agar pads, requiring lower doses to see the desired effects. Finally, this technique is advantageous for large-scale screens because it enables the use of automated liquid-handling systems for the high-throughput preparation of worm populations in multiwell plates.

10.3.2 *C. elegans* as a Model of Neurological Disease

Ongoing research with *C. elegans* has identified several genetic targets that have elucidated many biomolecular phenomena related to neuronal development and neurodegenerative disease [4, 5, 22]. The nematode is an excellent model organism for these investigations thanks to its simplicity and molecular similarity to higher-level organisms.

For instance, research focusing on *C. elegans* has aided in understanding the pathogenesis of protein misfolding in neurodegeneration. The major neurodegenerative diseases (Alzheimer's, Parkinson's, and Huntington's diseases) are all associated with abnormal protein folding and aggregation in the affected central nervous system (CNS) neurons, which eventually malfunction and degenerate [5, 23–25]. The molecular basis of these events is poorly understood. In the case of Huntington's disease, there is an inverse relationship between the length of an important glutamate chain in the Huntingtin protein and the age of onset of the disease. However, around a length of 42 glutamate residues, predicting the mechanism and likelihood of developing the disease is controversial [26]. Interestingly, researchers were able to transfect fluorescently tagged polyglutamine chains of various lengths into *C. elegans* body-wall muscle cells and observe the formation

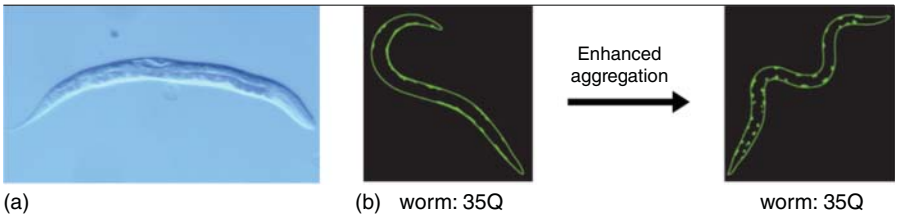

Figure 10.1 *C. elegans* as a model for studying neurodegenerative disease. (a) *C. elegans* has a nearly fully characterized genome and anatomy, and it is optically transparent. (b) Fluorescently tagged proteins aggregate under specific genetic conditions in a Huntington disease model. (Adapted with permission from Ref. [27], copyright Wiley-Blackwell and, copyright National Academy of Sciences U.S.A. 2004.)

of protein aggregates and behavioral declines (Figure 10.1) [27, 28]. This model served as a means to comprehensively probe the genetic basis of protein aggregation in Huntington's disease on a large scale. The study's findings further elucidated a relationship between aging on the onset of the misfolding in addition to the effect of the glutamine motif length.

C. elegans has also proven to be a good model for nerve regeneration after the invention of a precise laser injury method. Previously, such studies were limited to large animal models (rats, mice, and zebrafish) due to the lack of an adequate nerve injury method. In 2004, Adela Ben-Yakar's group demonstrated that femtosecond laser pulses could be used to study nerve regeneration in *C. elegans* [29]. By focusing these laser pulses to a very small focal volume inside *C. elegans* worms, it became possible to precisely cut motor neuron axons without damaging the surrounding tissue or bursting the cuticle. Interestingly, the injured neurons could spontaneously regenerate within 24 h of the laser axotomy, accompanied by functional recovery [29], while another study showed that other neurons close to the nerve ring could not regenerate at all [30].

The development of this laser axotomy technique spurred many studies to discover the role of multiple genes in axonal regeneration of *C. elegans* neurons [29, 31–37]. In two independent studies, the DLK-1 Map Kinase pathway was found to be critical for the development and proper regeneration of axons [32, 37]. Michael Bastiani's group performed an RNAi screen for genes modifying regeneration following spontaneous axon tears that formed as result of structural instability conferred by a mutation to the β-spectrin protein [32]. They then discovered that the DLK-1 map kinase pathway, which is conserved in humans, was necessary for proper regeneration following laser axotomy, independent of the effects of β-spectrin. Overactivity of this pathway led to overgrowth of axons and synapse morphology defects, while laser-cut axons could not regenerate as efficiently as axons in wild-type animals if one of the genes in the pathway was missing. In another study, Yishi Jin's group found that the DLK-1 pathway helps stabilize local mRNA translation along the axon during the regenerative process [37].

Yishi Jin's group undertook another major nerve regeneration investigation in which the researchers performed laser axotomies in 654 strains with mutations

in previously untested genes thought to play a role in the regenerative process [31]. Despite the unprecedented scale of this work, a large fraction of the worm's genome (more than 95%) still remains to be tested, which can realistically be achieved only by using high-throughput manipulation and imaging platforms. Automated microfluidic and optical technologies have begun to increase the throughput of such investigations and will enable genome-wide studies of neurodegenerative and regenerative phenomena in *C. elegans* [34, 38].

10.3.3 *C. elegans* as a Drug-Screening Model

With knowledge of its fully sequenced genome (up to 60% homology with vertebrates) [39–41] and easy cultivation in laboratory settings, *C. elegans* has become an emergent model for drug discovery related to human disease. Because much of the molecular machinery involved in these diseases is shared between the worm and humans, in many cases possible drug targets and interactions can be identified in worm assays [4, 8, 42–44]. In addition, its similarity to parasitic nematodes, which cause extensive harm to infected humans and devastate food supplies in resource-poor settings, makes *C. elegans* an intriguing organism to characterize nematode biology and develop antiparasitic agents [45, 46].

In fact, several antiparasitic compounds used to treat nematode infections in humans or kill agricultural pests were poorly understood until screens with *C. elegans* revealed genes in relevant neurotransmitter synthesis and processing pathways [22, 47–49]. In particular, the studies elucidated a genetic pathway necessary for proper synthesis and transport of nicotinic acetylcholine (nACh) in neurons and their synapses. In some cases, the mutations that the researchers discovered conferred resistance to the therapeutic compounds.

More than a dozen genetic markers directly related to human disease, including genes involved in the major neurodegenerative diseases, as well as diabetes and muscular dystrophy, have been extensively studied in *C. elegans* for drug discovery purposes [4]. In one study, the pharmaceutical company, Pfizer Inc. used *C. elegans* to screen 10 000 compounds to find suppressors of egg-laying defects linked to genes (*sel-12* and *egl*-36) that were orthologous to Alzheimer's markers [50]. The study relied on an automated fluorometric plate reader to measure the luminescent signal given by a chemical reporter of egg-laying volume. This research also demonstrated the convenience of high-throughput technologies when applied to *C. elegans* biology.

10.3.4 Current State of the Art in Automated *C. elegans* Screening

Thanks to their length scales and habituation to liquid environments, *C. elegans* are easily cultivated in multiwell plates coupled to robotic liquid-handling systems. These worms can be subsequently characterized in high-throughput optical sorting systems.

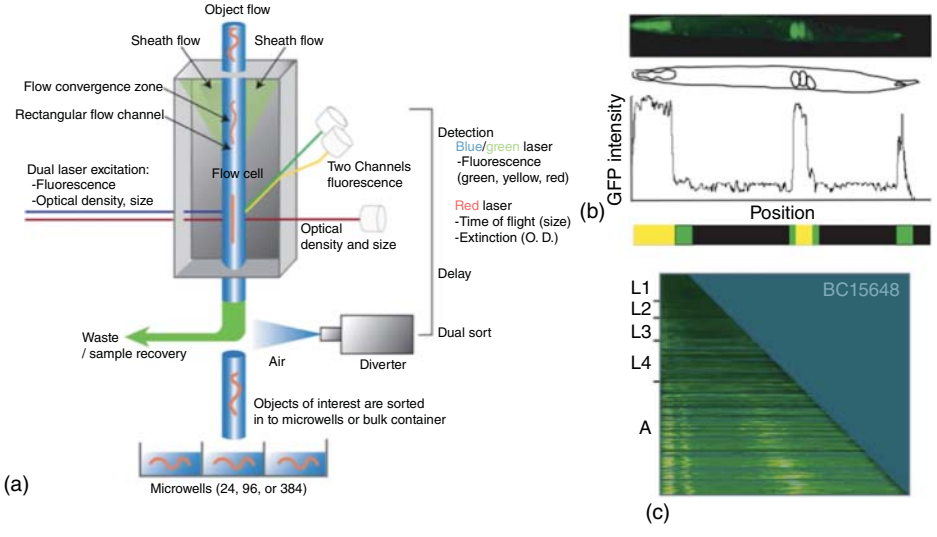

Figure 10.2 COPAS Biosort system as the current state of the art for automated *C. elegans*–screening systems. (a) The individual *C. elegans* worms (orange) are directed into the flow cell where optical density, body length, and overall multichannel fluorescence can be characterized to sort the animals in real time. (Adapted from Ref. [51], copyright Springer Publishing Company, with permission.) (b) Line-scanning optical data of integrated fluorescence along the anterior–posterior body axis can be obtained. (c) A condensed view of line scanning data of a given population sorted by life stage. (b and c are adapted from Ref. [52], copyright Nature Publishing Group 2007, with permission.)

The most advanced optical sorting system that is commercially available for screening *C. elegans* populations, is the COPAS Biosort (Figure 10.2). The system can optically scan many populations of worms to generate large-scale biological data sets [51–54]. This system has been used in several labs to perform screens where basic optical data could distinguish changes in gene expression to isolate mutants of interest or quantify spatiotemporal genetic phenomena [51]. The platform uses line-scanning measurements to give 1-D optical density, particle size, and multichannel fluorescence data from the long body-axis of each worm at a rate of 100 animals per second (Figure 10.2b).

Using the COPAS technology, Doitsidou *et al.* quantified overall GFP expression from dopaminergic neurons in a forward screen for genes that modify neuron morphology throughout the worm's body [53]. Though the sensitivity of this approach was lower than typical fluorescence microscopy techniques, the sheer number of animals screened per unit time on the COPAS system allowed the experimenters to identify mutants nearly seven times faster than conventional approaches. Another group used the COPAS system to generate data correlating developmental life stage with spatiotemporal gene expression along the worms' long body axis in strains with different GFP-tagged promoters (Figures 10.2b,c) [52]. They examined thousands of animals to understand the interactions between approximately 900 genes related to various aspects of the worm's physiology.

Expansions in the capabilities and applications of such automated sorting systems will accelerate the rate of research with *C. elegans* and help produce many insights into important biological phenomena. In some cases, relatively simple off-the-shelf technologies can be employed in an innovative manner to greatly simplify and accelerate *C. elegans* screens. For example, a recent study employed consumer flatbed scanners and novel image-processing techniques to perform a fully automated screen of lifespan on over 30 000 worms [55]. They placed several of the scanners in temperature-controlled incubators and periodically imaged approximately 800 agar plates in parallel. Analysis of subsequent images indicated if worms were viable or dead over the experimental time course. On a daily basis, the data acquired by a single flatbed scanner surpassed what one human researcher could collect within several hours.

Although they provide valuable insights, these optical interrogation platforms still have different pitfalls, such as the significant time bottleneck caused by slow population delivery mechanisms or limited precision and flexibility in automated optical interrogation and sample manipulation. Further technology development is needed to overcome these hurdles to provide a full range of novel automation and imaging capabilities that will enable ultrafast screening on the *C. elegans* nervous system. New sorting devices based on microfluidic technologies enabling higher specificity and resolutions have the potential to revolutionize drug discovery and high-throughput biology with this model organism. These developments make *C. elegans* an *in vivo* model with which to investigate complex biological phenomena at speeds and scales only previously achieved with simpler *in vitro* models.

10.4 Microfluidics

Microfluidics has become a ubiquitous tool in the chemical and life sciences over the last two decades, enabling automated manipulation of liquid samples at micron to nanometer length scales with unprecedented precision and throughput. The integration of these devices into various laboratory settings is enabling high-content experimentation in a repeatable and quantitative manner in molecular biology, chemistry, and medicine [56].

10.4.1 Microfluidic Device Fabrication

Early development of microfluidic devices focused on chips made from glass or silicon. Typically, wet etching or reactive ion etching (RIE) tools created channels of varying geometries in the substrate of choice for chemical analysis applications. These etching processes were both time consuming and resource intensive due to the need to perform lithography and etching with advanced machinery and harsh chemicals for every batch of devices made [57].

The pitfalls related to fabrication yield from using glass and silicon as a microfluidic substrate were overcome by a replica-molding approach pioneered by George Whitesides's group in 1998 [58, 59]. This technique became known as *soft-lithography* and is now the most common approach used to make microfluidic devices [56, 60]. This technique allows for the creation of micron-scale channels of arbitrary dimension and design on biocompatible elastomeric substrates, such as polydimethylsiloxane – PDMS, for a vast variety of specialized research applications.

In soft lithography, a pattern is typically defined in a photolithographic mask that is used to generate the same pattern in a photosensitive material (photoresist) that has been spin-coated onto a silicon wafer surface. The photoresist on silicon serves as the mold for an elastomer (e.g., PDMS) that is poured onto the wafer. The elastomer is then cured and removed from the wafer and the hardened piece bonds to a substrate, such as glass, silicon, or another piece of PDMS. The indentations left in the elastomer by the photoresist mold essentially become micron-scale fluid channels sealed from the external environment by the substrate bonded to the bottom of the new device or "microfluidic chip."

The second breakthrough in microfluidics came when Stephen Quake's group developed a method to fabricate two-layer microfluidic chips with unprecedented complexity and functionality, owed mainly to the integration of fully sealing on/off valves [17, 18]. At least two photoresist molds are needed to fabricate two microchannel layers for these chips. One of the layers has pneumatic inputs for the valve or membrane components of the chip, while the other channel layer usually houses the chemical or biological samples. For the bottom layer, PDMS elastomer is spin-coated across the mold so that a 20–30 μm layer of the material rests above the photoresist features. After the PDMS is hardened, the top layer of the device, which is usually fabricated as its own single layer in the typical fashion mentioned earlier, is bonded to the bottom layer. Both layers are then removed as one piece, which has fluidic access holes drilled into it. Finally, the entire two-layer elastomer chip is bonded to glass whose specifications match relevant optical system parameters.

10.4.2
Fluid Dynamics Modeling in Microfluidics

The development of microfluidic chips relies heavily on intuition and experience from testing and modifying the devices in conjunction with mathematical approaches from fluid mechanics. The intuitive approach is used to develop the basic conceptual chip design, while mathematical methods help in optimizing fluid flow profiles and flow rates.

The process of calculating the essential fluid flow characteristics for microfluidic systems can be accomplished by reducing the system to a fluidic circuit, as illustrated in Figure 10.3 [61]. The fluidic resistance of each major system component can be calculated based on their channel geometries. These resistances contribute to the total resistance of the microfluidic platform and can be combined together

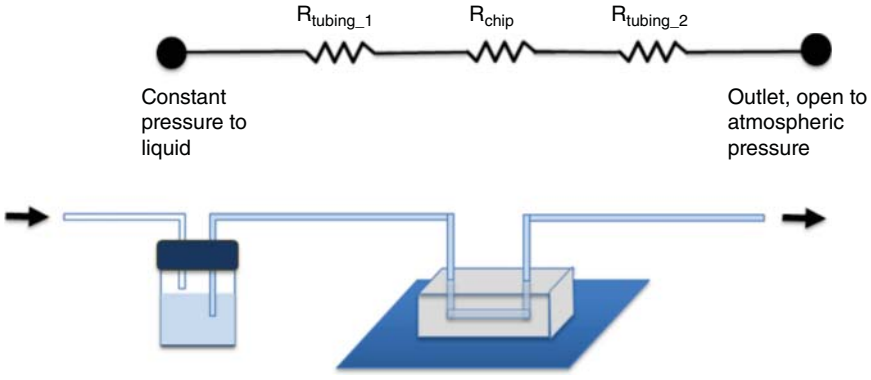

Figure 10.3 Microfluidic circuit model. A basic fluidic circuit model of a microfluidic system with flow driven by a constant pressure source. The fluidic resistances of the tubing before and after the chip are represented by R_{tubing} and the overall fluidic resistance of the microfluidic chip is represented by R_{chip}. A fluid source under constant gauge pressure (known) is fed to the chip from tubing and can then exit the chip through additional tubing to a lower pressure point (usually to atmospheric pressure).

in the same manner as the resistances of electrical circuit components. Based on the arbitrary pressure applied to the system's fluid reservoir, one can deduce flow rates, fluid velocities, and flow vector profiles at various points across the system with various analytical and numerical tools.

By applying the circuit model approach, one can use calculated fluidic resistance values and a given pressure applied at the fluid reservoir to deduce flow rates in the system using the following equation:

$$\Delta P = QR \tag{10.1}$$

where ΔP is the pressure drop across the channel, Q is the volumetric flow rate, and R is the fluidic resistance of the channel.

For the circular tubing connections, which externally interface into the microfluidic chips, the fluidic resistance can be estimated from the characteristic equations describing the fully developed laminar flow of an isothermal, incompressible, and isotropic Newtonian fluid in a tube with a circular cross-section and no-slip boundary condition on the sidewalls [62]:

$$R_{\text{tubing}} = \frac{128\mu L}{\pi d^4} \tag{10.2}$$

where L is the length of the tube, μ is the viscosity of the given fluid, and d is the diameter of the tube. The $1/d^4$ dependence of resistance on diameter makes even relatively small changes in diameter lead to vast changes in resistance.

The rectangular cross-sections typically seen inside microfluidic device channels require a modified formulation of fluidic resistance relative to the equation used for cylindrical channels (Eq. (10.2)). The rectangular fluidic resistance formulation comes from a solution of the Navier–Stokes equations following the

assumptions from Eq. (10.2) applied to the rectangular cross-section geometry. An analytical solution is given as [62]

$$R_{\text{chip}} = \frac{12\mu L}{wh^3}\left[1 - \frac{h}{w}\left(\frac{192}{\pi^5}\sum_{n=1,3,5}^{\infty}\frac{1}{n^5}\tanh\left(\frac{n\pi w}{2h}\right)\right)\right]^{-1} \tag{10.3}$$

where w is the smaller dimension between the width and height of the rectangular channel, while h is the larger dimension. All other variables are identical to their definitions in Eq. (10.2). For most microfluidic devices, the calculated resistance of the external tubing components are less than 0.1% of the fluidic resistance of the entire chip because of the relatively large diameter of tubings (0.5–2 mm) as compared with small cross-sectional dimensions of the devices' microchannels (1–500 μm):

$$R_{\text{tubing}} \approx 0.001 R_{\text{chip}} \tag{10.4}$$

When a detailed flow field is needed, one can model the flow in microchannels using a finite element multiphysics modeling software, such as COMSOL or Fluent. A microfluidic chip design can be imported into the software where different boundary conditions for either flow rate or pressure are applied throughout the device layout. The software can provide the fluid flow characteristics at each point in the device by numerically solving the conservation of mass and momentum equations for incompressible, laminar, and irrotational flow under steady-state conditions:

$$\begin{aligned} &\nabla \cdot u = 0 \\ &-\nabla \cdot \mu(\nabla u + (\nabla u)^T) + \rho(u \cdot \nabla)u + \nabla p = 0 \end{aligned} \tag{10.5}$$

where u is the flow velocity vector, μ is the viscosity, ρ is density, and p is pressure. If the layout of the microfluidic channel design has any geometric symmetry, the portion of the channel that repeats along the symmetry plane is sufficient to calculate the needed parameters. This approach drastically improves computational efficiency and duration.

Reynolds number is another important fluid mechanical parameter to consider in the design of microfluidic devices. This nondimensional parameter indicates the ratio between inertial forces and viscous forces acting on the fluid:

$$Re = \frac{d\rho u}{\mu} \tag{10.6}$$

where d is the characteristic length of the given channel, p is the density of the fluid, u is the average fluid velocity, and μ is the viscosity of the given fluid. Higher Reynolds numbers indicate that turbulence and enhanced mixing will occur in the fluid, while lower values indicate that sheaths of fluid flow moving in parallel inside a microchannel will not mix or travel in directions counter to the average fluid flow vector. At the lower Reynolds number regime ($Re = 0.1–100$), mixing of particles and molecules within the fluid occurs mainly through diffusion rather than chaotic mixing. This flow condition is called *laminar flow* and tends to dominate in microfluidic flow behavior [62].

10.4.3
Microfluidics Interfacing with Multiwell Plates

A major component of high-throughput bioassays is automated sample-processing and tracking. Well plates with multiple sample chambers are a common tool to simplify the housing and sorting of hundreds to thousands of samples within automated liquid-handling systems. Concurrently, microfluidic technology enables fast and automated control of chemical and biological samples with unprecedented complexity and precision inside a given device, but widespread adoption of this technology has been slowed by the lack of a simplified interface between the macroscale world and the devices' microchannels. Typically, several pneumatic and sample inputs on the chip must be coupled to individual syringes or pressurized sample reservoirs via tubing. These interfaces can be cumbersome and impractical, especially for labs with limited engineering expertise.

With this in mind, a few research groups and commercial entities have developed chips built into multiwell plates to facilitate delivery of samples to microfluidic channels where the chips' novel capabilities can be accessed and to make the devices amenable to automated plate-handling systems [63–65]. Essentially, a commercially available well plate with bottomless reservoirs or with laser-machined access holes is bonded on top of a thin PDMS microfluidic device layer such that each well plate reservoir is coupled to a single liquid input site on the chip or array of chips.

An example of a multiwell format microfluidic device for mammalian cell culture and screening is shown in Figure 10.4 [65]. These devices are then fastened into a gasket system or an automated plate-handling machine for manipulation of chemical and biological samples. Typically, most of these devices have a single continuous microchannel layer with various inputs, and the devices are used as cell culture bioreactors for different cell types. Most recently, we developed a device following the 96-well plate format with on-chip well reservoirs to further simplify the interface of the *C. elegans* populations with microfluidics, as described in a later section [66]. We now describe how to precisely manipulate individual samples via valve multiplexing, an approach that in combination with well plate-based devices can result in very robust and versatile capabilities.

10.4.4
Microfluidic Flow Control and Valve Multiplexing

Borrowing concepts from electrical engineering, researchers have applied multiplexing device logic to the design of microfluidic devices to greatly increase their capabilities. This approach necessitates much fewer on-chip valves than the total number of samples processed, without sacrificing the flexibility or precision manipulating the samples. With binary multiplexing (Figure 10.5), one regulates "n" separate sample channels with $2 \times \log_2(n)$ pneumatic microfluidic control valves (e.g., to regulate 384 channels, 18 valves are needed) [16, 18].

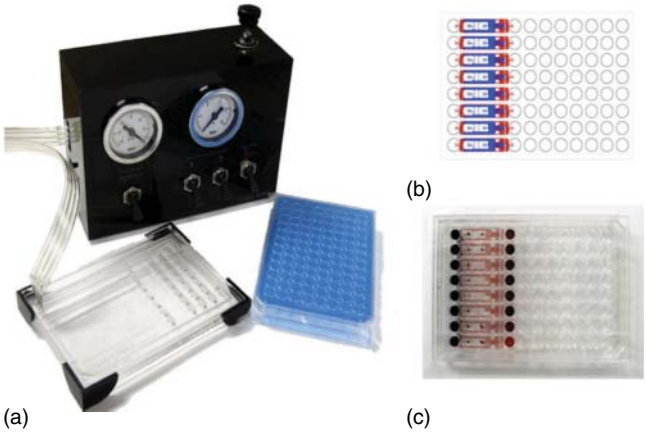

Figure 10.4 Microfluidic cell culture platform with an interface to multiwell plates. (a) The system includes a pneumatic regulation system (black box) coupled to a gasket that sits on top of the well plate format microfluidic chip interfacing with a commercially available 96-well plate (blue plate). (b) Schematic of the microchannels that interface with the well plate reservoirs. (c) The actual device with microchannels loaded with food coloring dye. (Adapted with permission from Ref. [65], copyright Sage Journals 2007.)

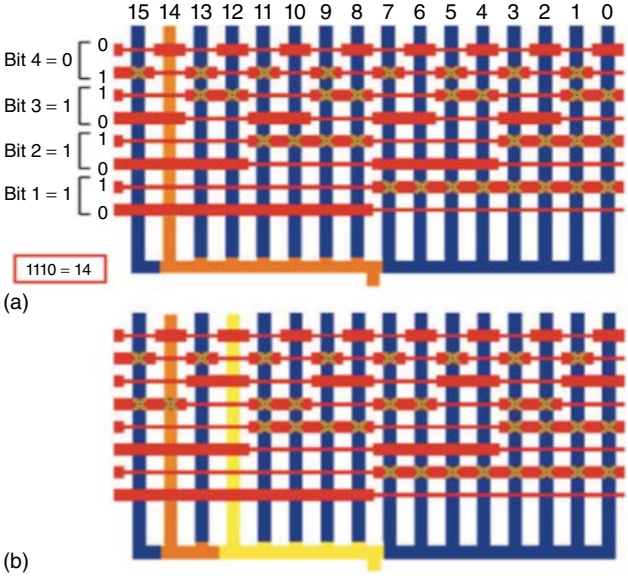

Figure 10.5 A binary microfluidic valve multiplexing. Here "*n*" samples are regulated by $2 \times \log_2(n)$ control valves. (a) The orange sample is delivered to the common outlet by opening and closing a precise set of control valves. (b) The yellow sample can be subsequently delivered by switching on/off positions between just two valves. (Adapted from Ref. [16], copyright Annual Reviews of Biotechnology 2007, with permission.)

Another research group developed a combinatorial multiplexer scheme that improved the ratio of samples controlled to total valves, with "N" control valves to regulating $N!/(N/2)!^2$ sample channels (e.g., to regulate 384 channels, 11 valves are needed) [67].

So far, microfluidic devices with multiplexed valve control have been geared toward handling liquid compounds in chemical, biochemical, and cell-based studies [17, 18, 67–70]. One research group suggested that microfluidic multiplexing could be a means to send different chemicals from standard well plates to single *C. elegans* worms inside a chip as a means to automate the animal's exposure to multiple conditions [71]. Yet, these large, freely moving animals can move unpredictably relative to the consistent laminar flow profiles in microfluidic chips, complicating the actual transport of large populations of *C. elegans* inside these devices for large-scale automated screens.

The Ben-Yakar group recently developed a microfluidic platform to automatically deliver multiple live populations of large-sized microorganisms (e.g., cell clusters, nematodes, drosophila, and zebrafish larvae) at high speeds [66]. This system addresses the complications of repeatedly transporting populations of motile animals without harmful anesthetics inside the microchannels, as discussed later in this chapter. By dramatically shortening the delivery time from the macroworld to a given microfluidic device, the system eliminates a major bottle neck facing large high-throughput screens with *C. elegans.*

10.5 Microfluidics for *C. elegans* Biology

With the apparent capabilities provided by microfluidic devices in regard to manipulating microscopic samples in an automated and precise fashion, the *C. elegans* research community has gradually adopted this technology to increase throughput and repeatability in various biological studies. The worm's body length scales (~10 to 70 μm × ~250 to 1000 μm) and simple culturing conditions make it an obvious target for microfluidic applications [9, 20, 72]. We now describe a few novel systems designed to enhance neurobiology investigations and high-throughput drug and genetic screens with the worm.

10.5.1 Microfluidic Worm Immobilization and High-Resolution Optical Interrogation Platforms

Although capable of obtaining optical information on a large number of worms in a very short time period, systems such as the COPAS Biosort and the flatbed scanner array described earlier do not yield high-resolution and detailed imaging data, nor do they precisely perturb the animals in a high-throughput fashion. Several labs, including our own research group, have been developing optical imaging and manipulation platforms for *C. elegans* bioassays with microfluidic approaches [34, 38, 66, 71, 73–104]. In general, microfluidic trapping devices either

immobilize worms one at a time or multiple worms simultaneously. In the multitrapping devices, multiple animals can be trapped simultaneously and processed either in series or simultaneously for the analysis of development, behavior, and life span, as examples [76, 77, 82, 88, 89, 97, 101]. Serial processing chips can trap the animals one-by-one for high-resolution imaging, sorting, or optical manipulation for various applications and transport them to a different off/on-chip location if further analysis is needed [34, 71, 79–81].

10.5.1.1

Single Trap Microfluidic Platforms for Worm Processing One at a Time

Single worm trapping is useful for various studies involving phenotyping, sorting, laser nanosurgery, and behavioral assays. These assays usually require high-resolution imaging and manipulation of a large number of worms in a serial manner, and thus worms must be placed in a precise orientation relative to the platform's optical interface in a repeatable manner. In addition, this level of precision may necessitate an immersion objective with a large numerical aperture ($NA > 1.2$) to image through a thin glass interface. Since these glasses can be very fragile, the device dimensions would be limited to sizes that do not strain and break the glass during routine handling.

In the last decade, there have been various microfluidic immobilization methods presented in the *C. elegans* literature. These devices typically involve mechanical trapping and manipulation assisted by either tapered channels [74], pressurized membranes to immobilize single worms [34, 71, 80, 81], small suction channels to grab single animals from a population [80], the application of CO_2 [104], or cold fluid (4 °C) [79, 91] to induce temporary paralysis, applied electric fields to induce electrotaxis [100], or surface acoustic wave perturbation [92].

The majority of these devices operate in a serial manner using precisely timed actuation of off-chip solenoid valves to activate on-chip membrane valves to control the transport of worms in the channels, such that a large number could be sequentially studied with various optical methods. This "one-by-one" approach requires only one imaging/interrogation area to receive single worms, which are subsequently either discarded after interrogation or transported to another location on-chip or to an external storage platform as the next worm arrives for optical interrogation.

One of the earliest applications of microfluidics for trapping single *C. elegans* animals comes from Cornelia Bargmann's group [74]. Their single-layer device consists of a small channel that tapers in width such that the animal could be trapped while its mouth protrudes partially into a perfusion chamber (Figure 10.6a). Various fluidic inputs deliver buffers and chemical stimuli to the worm's head to allow correlation of fluorescent calcium transients in chemosensory neurons with the onset and removal of the stimulus. This device is relatively simple but is a powerful tool to enable the acquisition of meaningful *in vivo* data from worms by eliminating the need for intrusive and harmful anesthetic agents to immobilize the animals.

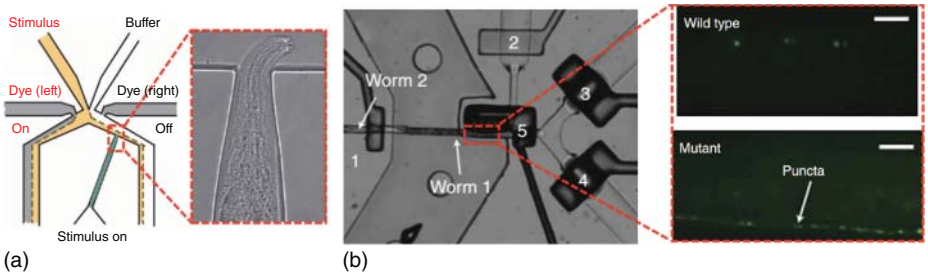

Figure 10.6 Examples of single trap microfluidic devices for serially processing *C. elegans*. (a) A single-layer device with a tapered channel for characterizing neuronal responses to different chemical stimuli. (Adapted from Ref. [74], copyright the Nature Publishing Group, with permission.) (b) A double-layer device for imaging-based phenotypic screens (picture on the left). On the right, fluorescence images of wild-type and mutant synapse phenotypes that the system used as its sorting criteria (scale bar ~10 μm). (Adapted from Ref. [79], copyright Nature Publishing Group 2008, with permission.)

Using a fluorescence microscope, Hang Lu's group developed a serial-processing microfluidic device that sent hundreds of worms per hour to an imaging channel where they could be imaged and sorted based on different phenotypic criteria (Figure 10.6b) [79]. The chip has two channel-layers, with one layer consisting of on-chip valves to control flow of fluid and samples in the other channel layer. The system also uses a novel temperature-based immobilization technique to keep worms still enough for high-resolution imaging. Custom software utilizes image-processing algorithms to sort the worms based on thresholds of fluorescence intensity of specific chemosensory neurons under different genetic backgrounds. The same research group later developed an improved version of this platform and implemented advanced machine learning algorithms to automatically find faint changes in neuronal synapse formation [91]. This approach identified several new genes related to synaptogenesis with unprecedented speed and accuracy.

Researchers also made significant strides to utilize serial microfluidics to facilitate laser-mediated nerve regeneration studies with *C. elegans.* Adela Ben-Yakar's group designed and fabricated a two-layer lab-on-chip platform including an immobilization chamber for precise axotomy on worms and recovery chambers to house the animals for follow up on their regenerating axons (Figure 10.7) [81]. To immobilize the worms, pressure is applied in the second channel layer, which is pneumatically linked to the deformable membrane above the immobilization chamber. This actuation collapses the membrane onto the worm and presses its body against the cover slip below (Figure 10.7a). This orientation provides ideal optical access to neurons of interest. Studies with the device revealed that axonal regrowth in mechanosensory neurons was much faster (~60 to 90 min, Figure 10.7c) when worms were processed on chip, as opposed to those mounted on agar pads with anesthetics (~6 to 12 h) [81].

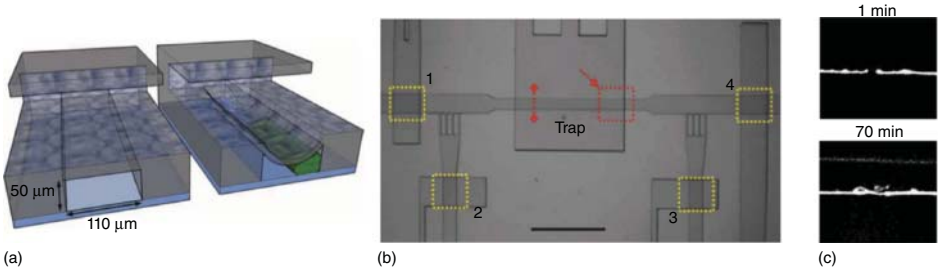

Figure 10.7 The laser axotomy chip for imaging, laser nanoaxotomy, and housing of *C. elegans*. (a) Conceptual three-dimensional section renderings of the bilayer trap channels without and with a worm (green) immobilized by a membrane. (b) View of the trapping system: Valves 1–4 (yellow rectangles) respectively control inlet regulation (1), fine positioning of the worm (2 and 3), and gating to the recovery chambers (4) (scale bar ~1 mm). (c) A fluorescence image of the mechanosensory neuron axon immediately after laser axotomy (1 min) and after reconnecting across the cut site (70 min). (Adapted with permission from Ref. [81], copyright Nature Publishing Group 2008.)

In a parallel effort, Fatih Yanik's group developed similar devices for performing laser axotomy and two-photon imaging studies of nerve regeneration in *C. elegans* [34, 71, 80]. With one such platform, they performed a large-scale screening to identify chemical compounds affecting neurite regrowth after axotomies to mechanosensory neurons [34]. To simplify the transport and handling of different worm populations to the device, they coupled the chip's entrance to tubing that would extract the worms from multiwell plates, instead of delivering them via syringe (Figure 10.8a). This delivery method, together with semi-automated manipulation of worms decreases the time and effort needed to perform the

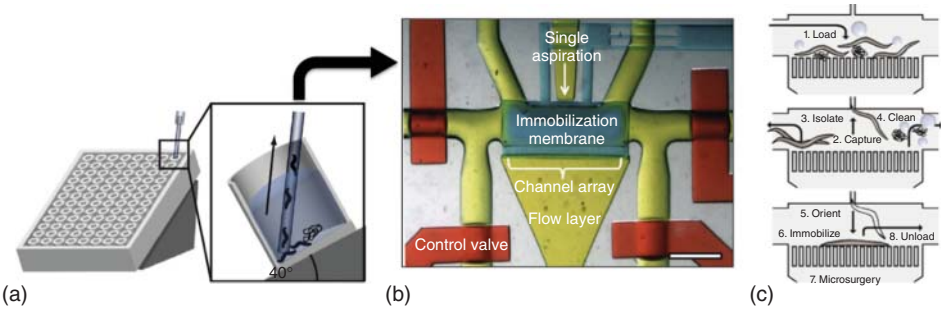

Figure 10.8 Screening chemical modulators of axonal regrowth in a microfluidic chip. (a) A multiwell plate is seated on an angled stand to condense the worm populations in a corner of the well from which they can be delivered to the device. (b) The microfluidic device with key components of the immobilization area filled with different food-coloring dyes. (c) A few worms are delivered to the device, where a single animal is trapped and immobilized for axotomy and imaging after cleaning steps. (Adapted with permission from Ref. [34], copyright National Academy of Sciences U.S.A. 2010.)

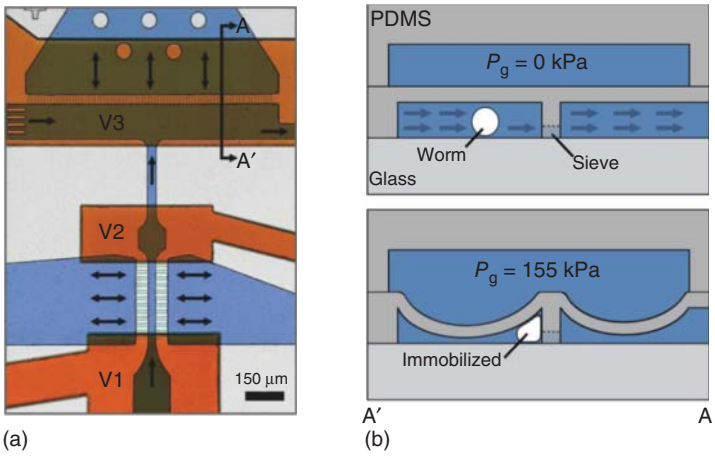

Figure 10.9 A fully automated serial laser nanoaxotomy platform. (a) Optical image of a dye-filled microfluidic device with black arrows indicating the direction of fluid flow. Orange dye fills the control layer and the blue dye identifies the flow channels. The loading chamber holds preloaded worms before their serial transportation into the staging and T-shaped immobilization area (A–A′). (b) Schematic cross-section referring to the sectioning arrows A–A′ in (a) that shows the flow direction through the sieves before membrane deflection, the location of the worm in the trapping area during delivery and after membrane deflection, and the relative heights of the microfluidic sieve and channel within the immobilization zone. (Adapted with permission from Ref. [38], copyright Public Library of Science 2014.)

screen. Their studies revealed specific chemical modulators of neurite regrowth in the PLM mechanosensory neuron.

The aforementioned laser axotomy systems both require human user intervention to precisely define the axotomy cut site inside each worm. To enable high-throughput automated studies of nerve regeneration in *C. elegans*, Adela Ben-Yakar's group enhanced their microfluidic device (Figure 10.9) and developed an image processing system to enable fully automated processing and laser surgery on worms in a serial manner. The custom image-processing algorithms automatically identified if a worm was in the imaging chamber, found the neuron of interest, targeted its axon, and finally performed laser axotomy using high-resolution optics [38]. A population of worms entered a loading chamber where a sequence of flow and valve inputs were actuated to move individual worms one at a time to a staging area (the channel between valves V1 and V2, Figure 10.9a). Small sieve structures in the staging area allowed fluid to pass without losing the worms. Flow was then reversed across the sieves in the staging area to quickly deliver the staged worm to a T-shaped immobilization chamber (below valve V3, Figure 10.9a). This T-shape orientation enabled the straightening of the worm body against the sidewall with sieve structures (Figure 10.9b). At this point, a membrane was pressurized to immobilize the animal. The entire process, including automated targeting and axotomy in the neuron of interest only required

approximately 17 s per worm, culminating in an unprecedentedly fast and fully automated subcellular ablation system for *in vivo* nerve regeneration studies.

In summary, serial processing devices allow fast perturbation and acquisition of the relevant biological data. Bringing the animals to a single location with the necessary optical and environmental conditions fixed, facilitates sequential investigation of tens to thousands of animals in a repeatable manner, all within a short period of time. However, in serial devices with two layers, the constant actuation of valves and fluid flow inputs could lead to mechanical failures that would not be encountered as often on more passively operating devices. Single-layer devices are less prone to these issues, but they may lack the versatility afforded by on-chip valves. Overall, single trap devices streamline the workflow by having one location for data acquisition and simplify device optimization since one must only improve one sample-processing element. There is no need to consider the simultaneous interactions between many trapping or housing elements in the device.

10.5.1.2

Multitrap Microfluidic Platforms to Enable Parallel Worm Processing

Another route to high-throughput studies of *C. elegans* worms on-chip is parallelization of a number of trapping channels. In this approach, the number of channels for immobilization, imaging, and surgery could be increased to tens to hundreds of channels in the device design and arranged in a parallel fluidic circuit. Thus, one could simultaneously load and house many worms from a single population in their own individual imaging and surgery chambers in a single device. For lower resolution and magnification phenotyping screens, these devices afford simultaneous imaging of multiple worms. Being primarily single-layer devices, this class of platforms affords relatively simple fabrication and device operation [74, 77]. An on-chip valve system can further improve the performance by enabling more precise control of sample manipulation, which makes the sample positioning more repeatable for automated imaging [34, 38, 79, 81, 84].

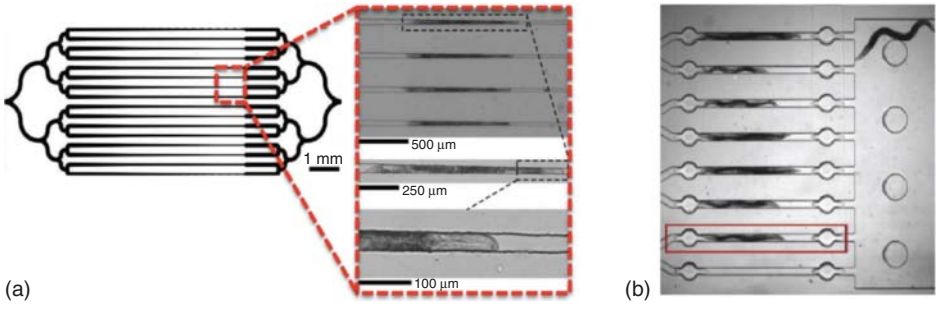

Figure 10.10 Multitrap microfluidic devices for parallel or serial processing of *C. elegans*. (a) A single-layer device with channels that taper to a minimal width that are arranged in parallel to trap several worms for various imaging studies. (Adapted from Ref. [77], copyright the Royal Society of Chemistry 2007, with permission.) (b) A double-layer device with membrane valves that flank worms loaded into thin channels arranged in parallel. (Adapted from Ref. [102], copyright Elsevier 2010, with permission.)

A couple of research groups introduced simple microfluidic devices that utilize parallelization in their designs. A single-layer device from George Whiteside's group had a single inlet, which bifurcated seven times to create 2^7 (128) trapping channels that taper in width over a length of 5 mm from 100 μm down to 10 μm (Figure 10.10a) [77]. The same group adapted a similar design to a device that could immobilize and house several worms for analysis of development during the animals' lifespans [88]. Single animals are immobilized in one of these tapering regions and block most of the flow through that particular channel, such that the likelihood of another worm entering that location is much lower than the probability of it following the upstream bifurcations to another open trapping channel. While the bifurcations limit worms from overfilling single channels, they necessitated a 15–20 min loading time to fill the traps. Allen *et al*. developed a chip that consisted of an array of tapering trapping channels in parallel placed downstream of a worm-loading inlet channel [98]. Similar to the channels in the previous device, the 5 mm long trapping channels are 100 μm wide at their entrance and 8 μm at their opposite end, which is a small enough width to prevent the animals from squeezing through. Once a worm entered the trap, it blocks flow sufficiently to prevent another worm from entering the same trap in the majority of cases. Both of these devices require constant applied pressure to the inlet channel to guarantee long-term immobilization of animals. In an example of this parallelized approach, Lockery and colleagues created a device with integrated electrodes to simultaneously measure pharyngeal pumping rates in several worms responding to antiparasitic compounds [83].

Another work from Hang Lu's group demonstrated a two-layer device to trap multiple worms in parallel and automatically induce synaptic transmission via parallel photonic activation of light-sensitive ion channels expressed in specific neurons (Figure 10.10b) [102]. This chip has membrane valves at opposite sides of eight individual traps that would actuate simultaneously to allow worms to enter and exit the device's imaging area. The system simultaneously obtained video of all eight animals before, during, and after the stimulus, which allowed deduction of their motility response from image-processing algorithms applied to the data after the experiment.

A main advantage of parallelization versus the serial-handling approach in single trap chips is that the worms can remain housed in their imaging and surgery chambers between observations. This aspect is especially important for studies requiring monitoring for a long period of time, such as aging and nerve regeneration studies. Housing the worms in parallel avoids repeatedly moving single worms out of the imaging and surgery portion of the chip for high-volume experiments. Furthermore, the complexity of automating on-chip flow and valve actuation, in addition to the time spent transporting animals through the device are greatly reduced with the proper approach. The primary disadvantage of this strategy is that to study hundreds or thousands of worms, a large-area chip (several centimeters in diameter) would be needed. Fabrication of larger area microfluidic devices with two channel-layers requires more precise alignment of the valve control layer with respect to the fluid channel layer. In addition, the complex sorting

procedures that one could perform in single trap devices is much less feasible in the multitrap platforms. Finally, automated studies would necessitate a motorized translation stage for optical observations of different immobilization chambers.

In summary, multitrap worm chips can simultaneously transport, isolate, and immobilize many worms, reducing overall workflow duration relative to devices that perform all of these processes in series. However, the requirement to increase the number of individual chambers for each animal studied to enhance throughput can lead to larger device footprints and the need for an automated data acquisition platform with high-resolution translation stages and autofocusing. Consequently, imaging applications with high-resolution oil or water immersion objectives can also add complications to the imaging process, but can perform with these capabilities at unprecedented speeds. In these devices, housing worms on-chip for long periods will also require extensive characterization of potential biological perturbations caused by the microfluidic environment, such as nutrient transport and cross-contamination between samples that have been exposed to different chemical conditions.

10.5.2 Microfluidic Population Delivery for Serial Processing

For large genome-wide screens across several distinct animal populations, the accuracy and speed of automated population-handling plays a critical role in the given study's success. For instance, the COPAS Biosort system (Figure 10.2) receives multiple populations of *C. elegans* worms from multiwell plate reservoirs using an automated, macroscale delivery system. This system utilizes a mechanical suction apparatus to transport the animals from well plates to the imaging hardware via tubing, a process that lasts approximately 45 s per population. This timing is needed to remove the bubbles introduced to the sample when the tubing is periodically exposed to the open environment. The bubbles may obstruct the field of view for imaging and generate artifacts in high-throughput data collection. This cleaning step makes the sample delivery time last more than an order of magnitude longer than the actual data collection steps. A significant reduction in the time needed for bubble-free delivery for each population would dramatically shorten the time needed for a large-scale drug screen.

With microfluidic devices, automated population handling can also greatly enhance throughput. In the aforementioned microfluidic immobilization platforms, one must manually send each population into the chip via syringe. While this method requires very simple tools and approaches, the process can be very cumbersome and time-consuming. Syringes require milliliter volumes to address the nanoliter volumes of microfluidic channels and often introduce bubbles to the devices. These restrictions lead to overuse of reagents and excessive effort to prepare each population for screening. Attempts have been made to circumvent these problems. A mechanical suction method analogous to the COPAS system's delivery technology was adapted to transport *C. elegans* from well plates to a microfluidic device built for laser axotomies [34]. However, bubble and debris

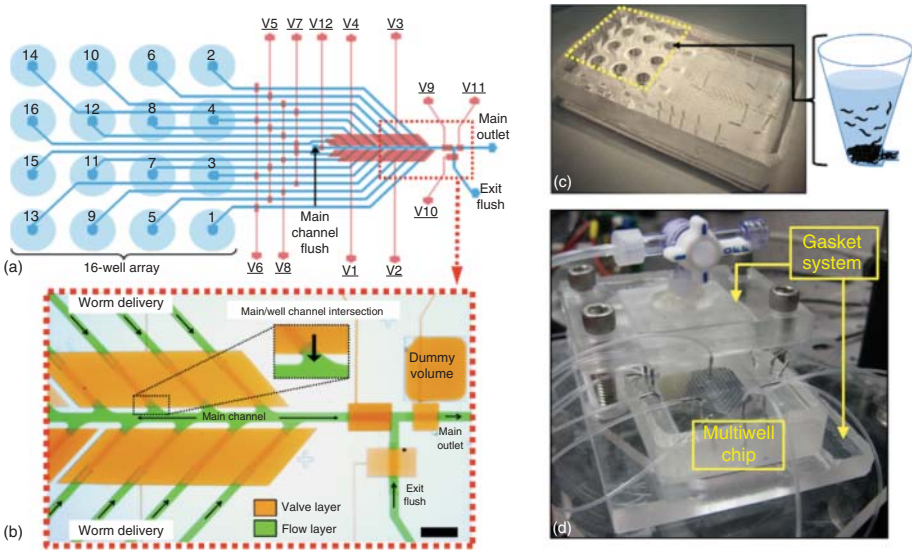

Figure 10.11 *Population delivery chip.* (a) A schematic of the device indicating the flow layer (blue) and control valve layer (red). There are 16 on-chip wells arranged in a 96-well plate format for initial loading of different worm populations. Columns and wells of the array are numbered according to order of delivery. Valves V1–V8 are multiplexer control valves and V9–V12 control flow in the main channel. (b) An image of the device with its microfluidic channels loaded with food-coloring dye, showing the flow layer (green) and control valve layer (orange) (scale bar ~1 mm). (c) A macroscale view of the device with the 16-well array indicated by the yellow dashed lines and a schematic of worms loaded into one of the conical wells. (d) A macroscale view of the entire chip/gasket system with pressurized input lines in the experimental setup. (Adapted from Ref. [66], copyright Public Library of Science 2013.)

contamination was frequent, necessitating washing steps on-chip for each worm surgery, as shown in Figure 10.8b.

To circumvent the pitfalls of these macro-scale (manual or automated) population-handling modalities, Ben-Yakar's group recently developed a microfluidic multiplexing device to deliver *C. elegans* populations to downstream imaging platforms (Figure 10.11) [66]. This *Population Delivery Chip* has an array of 16 on-chip well reservoirs arranged in a 96-well plate format and an on-chip multiplexed valve system that addresses each of these reservoirs. The automated platform achieves delivery of approximately 90% of the worms loaded in each well population in less than 5 s per population without cross-contamination between wells or harming animal viability. This delivery speed is an order of magnitude faster than the COPAS system's delivery mechanism. The all-fluid interfaces enabled by the design and the gas-permeability of PDMS eliminated the introduction of bubbles to the delivered samples. In addition, the on-chip, multiwell format reservoirs provide a simplified interface to load worms into the device microchannels. Larger-scale systems with dozens to hundreds of

populations are in development and will significantly boost throughput for various *C. elegans* screening applications with microfluidics.

Such a population delivery device can be coupled to downstream imaging platforms, including microfluidic devices and flow cell imagers, culminating in increasingly integrated systems and fully automated high-throughput screens. Furthermore, using the capabilities of various optical systems, such as high-resolution imaging/ablation and automated image processing, researchers will obtain rich data sets with unprecedented speed. To maximize the utility of these technologies, mature and robust iterations of the microfluidic system hardware must be built to sustain the multi-hour and multi-day screens. Image-processing and machine-learning algorithms will enhance the automation and decrease user intervention during data acquisition, while massively parallel computing systems may be needed to process and interpret the large imaging data sets that are collected by these systems.

10.6 Conclusions and Future Directions

The flexibility in design and engineering of microfluidics coupled with the biological significance and utility of *C. elegans* have enabled extraordinary developments in high-throughput biological assay platforms to study *in vivo* phenomena. As current device platforms are optimized and new ones emerge, increasing numbers of biologists will be able to spend less time manually manipulating individual worms or populations of worms and will instead focus on designing new assays for the automated microfluidic platforms, subsequently obtaining and analyzing relevant data in larger volumes. As these technologies accelerate research with *C. elegans*, our understanding of fundamental biomolecular phenomena will expand in multiple areas, while upstream drug development pipelines will shorten.

Author Contributions

N.G., S.K.G., and A.B.-Y. prepared the manuscript. They declare no conflicts of interest.

References

1. Insel, T. (2008) Assessing the economic costs of serious mental illness. *Am. J. Psychiatry*, **165**, 663–665.
2. Kessler, R.C., Heeringa, S., Lakoma, M.D., Petukhova, M., Rupp, A.E., Schoenbaum, M. *et al.* (2008) The individual-level and societal-level effects of mental disorders on earnings in the United States: results from the National Comorbidity Survey Replication. *Am. J. Psychiatry*, **165**, 703.
3. Fang, Y. and Bonini, N.M. (2012) Axon degeneration and regeneration: insights from *Drosophila* models of nerve injury. *Annu. Rev. Cell. Dev. Biol.*, **28**, 575–597.

4. Kaletta, T. and Hengartner, M.O. (2006) Finding function in novel targets: *C. elegans* as a model organism. *Nat. Rev. Drug Discovery*, **5**, 387–399.
5. van Ham, T.J., Breitling, R., Swertz, M.A., and Nollen, E.A. (2009) Neurodegenerative diseases: lessons from genome-wide screens in small model organisms. *EMBO Mol. Med.*, **1**, 360–370.
6. Hammarlund, M. and Jin, Y. (2014) Axon regeneration in *C. elegans*. *Curr. Opin. Neurobiol.*, **27**, 199–207.
7. Antoshechkin, I. and Sternberg, W. (2007) The versatile worm: genetic and genomic resources for *Caenorhabditis elegans* research. *Nat. Rev. Genet.*, **8**, 518–532.
8. Hulme, S.E. and Whitesides, G.M. (2011) Chemistry and the worm: *Caenorhabditis elegans* as a platform for integrating chemical and biological research. *Angew. Chem. Int. Ed.*, **50**, 4774–4807.
9. Hulme, S.E., Shevkoplyas, S.S., and Samuel, A. (2008) Microfluidics: streamlining discovery in worm biology. *Nat. Methods*, **5**, 589–590.
10. Han, M. (2010) Advancing biology with a growing worm field. *Dev. Dyn.*, **239**, 1263–1264.
11. Breslauer, D.N., Lee, J., and Lee, L. (2006) Microfluidics-based systems biology. *Mol. Biosyst.*, **2**, 97–112.
12. Kim, S., Streets, A.M., Lin, R.R., Quake, S.R., Weiss, S., and Majumdar, D.S. (2011) High-throughput single-molecule optofluidic analysis. *Nat. Methods*, **8**, 242–245.
13. Martin, L., Meier, M., Lyons, S.M., Sit, R.V., Marzluff, W.F., Quake, S.R. *et al.* (2012) Systematic reconstruction of RNA functional motifs with high-throughput microfluidics. *Nat. Methods*, **9**, 1192–1194.
14. White, A.K., VanInsberghe, M., Petriv, I., Hamidi, M., Sikorski, D., Marra, M.A. *et al.* (2011) High-throughput microfluidic single-cell RT-qPCR. *Proc. Natl. Acad. Sci. U.S.A.*, **108**, 13999–14004.
15. Lecault, V., VanInsberghe, M., Sekulovic, S., Knapp, D.J., Wohrer, S., Bowden, W. *et al.* (2011) High-throughput analysis of single hematopoietic stem cell proliferation in microfluidic cell culture arrays. *Nat. Methods*, **8**, 581–586.
16. Melin, J. and Quake, S.R. (2007) Microfluidic large-scale integration: the evolution of design rules for biological automation. *Annu. Rev. Biophys. Biomol. Struct.*, **36**, 213–231.
17. Unger, M.A., Chou, H., Thorsen, T., Scherer, A., and Quake, S.R. (2000) Monolithic microfabricated valves and pumps by multilayer soft lithography. *Science*, **288**, 113–116.
18. Thorsen, T., Maerkl, S.J., and Quake, S.R. (2002) Microfluidic large-scale integration. *Science*, **298**, 580–584.
19. Brenner, S. (1974) The genetics of *Caenorhabditis elegans*. *Genetics*, **77**, 71–94.
20. Riddle, D., Blumenthal, T., Meyer, B., and Priess, J. (1997) *C. elegans II. Plainview*, vol. 4, Cold Spring Harbor Laboratory Press, New York, p. 2006, Retrieved April.
21. Stiernagle, T. (2006) *Maintenance of C. elegans*. *WormBook*, **11**, 1–11.
22. Jones, A.K., Buckingham, S.D., and Sattelle, D.B. (2005) Chemistry-to-gene screens in *Caenorhabditis elegans*. *Nat. Rev. Drug Discovery*, **4**, 321–330.
23. Masters, C., Simms, G., Weinman, N., Multhaup, G., McDonald, B., and Beyreuther, K. (1985) Amyloid plaque core protein in Alzheimer disease and Down syndrome. *Proc. Natl. Acad. Sci. U.S.A.*, **82**, 4245–4549.
24. Scherzinger, E., Lurz, R., Turmaine, M., Mangiarini, L., Hollenbach, B., Hasenbank, R. *et al.* (1997) Huntingtin-encoded polyglutamine expansions form amyloid-like protein aggregates in vitro and in vivo. *Cell*, **90**, 549–558.
25. Singleton, A.B., Farrer, M., Johnson, J., Singleton, A., Hague, S., Kachergus, J. *et al.* (2003) alpha-Synuclein locus triplication causes Parkinson's disease. *Science*, **302**, 841.
26. Brinkman, R., Mezei, M., Theilmann, J., Almqvist, E., and Hayden, M. (1997) The likelihood of being affected with Huntington disease by a particular age,

for a specific CAG size. *Am. J. Hum. Genet.*, **60**, 1202–1210.
27. Nollen, E.A., Garcia, S.M., van Haaften, G., Kim, S., Chavez, A., Morimoto, R.I. *et al.* (2004) Genome-wide RNA interference screen identifies previously undescribed regulators of polyglutamine aggregation. *Proc. Natl. Acad. Sci. U.S.A.*, **101**, 6403–6408.
28. Morley, J.F., Brignull, H.R., Weyers, J.J., and Morimoto, R.I. (2002) The threshold for polyglutamine-expansion protein aggregation and cellular toxicity is dynamic and influenced by aging in *Caenorhabditis elegans*. *Proc. Natl. Acad. Sci. U.S.A.*, **99**, 10417–10422.
29. Yanik, M.F., Cinar, H., Cinar, H.N., Chisholm, A.D., Jin, Y., and Ben-Yakar, A. (2004) Neurosurgery: functional regeneration after laser axotomy. *Nature*, **432**, 822.
30. Chung, S., Clark, D., Gabel, C., Mazur, E., and Samuel, A. (2011) The role of the AFD neuron in *C. elegans* thermotaxis analyzed using femtosecond laser ablation. *BMC Neurosci.*, **7**, 30.
31. Chen, L., Wang, Z., Ghosh-Roy, A., Hubert, T., Yan, D., O'Rourke, S. *et al.* (2011) Axon regeneration pathways identified by systematic genetic screening in *C. elegans*. *Neuron*, **71**, 1043–1057.
32. Hammarlund, M., Nix, , Hauth, L., Jorgensen, E.M., and Bastiani, M. (2009) Axon regeneration requires a conserved MAP kinase pathway. *Science*, **323**, 802–806.
33. Pinan-Lucarre, B., Gabel, C., Reina, C., Hulme, S., Shevkoplyas, S., Slone, R. *et al.* (2012) The core apoptotic executioner proteins CED-3 and CED-4 promote initiation of neuronal regeneration in *Caenorhabditis elegans*. *PLoS Biol.*, **10**, e1001331.
34. Samara, C., Rohde, C.B., Gilleland, C.L., Norton, S., Haggarty, S.J., and Yanik, M.F. (2010) Large-scale *in vivo* femtosecond laser neurosurgery screen reveals small-molecule enhancer of regeneration. *Proc. Natl. Acad. Sci. U.S.A.*, **107**, 18342–18347.
35. Wang, Z. and Jin, Y. (2011) Genetic dissection of axon regeneration. *Curr. Opin. Neurobiol.*, **21**, 189–196.
36. Wu, Z., Ghosh-Roy, A., Yanik, M.F., Zhang, J.Z., Jin, Y., and Chisholm, A.D. (2007) *Caenorhabditis elegans* neuronal regeneration is influenced by life stage, ephrin signaling, and synaptic branching. *Proc. Natl. Acad. Sci. U.S.A.*, **104**, 15132–15137.
37. Yan, D., Wu, Z., Chisholm, A.D., and Jin, Y. (2009) The DLK-1 kinase promotes mRNA stability and local translation in *C. elegans* synapses and axon regeneration. *Cell*, **138**, 1005–1018.
38. Gokce, S.K., Guo, S.X., Ghorashian, N., Everett, W.N., Jarrell, T., Kottek, A. *et al.* (2014) A fully automated microfluidic femtosecond laser axotomy platform for nerve regeneration studies in *C. elegans*. *PLoS One*, **9**, e113917.
39. Harris, T.W., Chen, N., Cunningham, F., Tello Ruiz, M., Antoshechkin, I., Bastiani, C. *et al.* (2004) WormBase: a multi-species resource for nematode biology and genomics. *Nucleic Acids Res.*, **32**, D411–D417.
40. Sonnhammer, E.L. and Durbin, R. (1997) Analysis of protein domain families in *Caenorhabditis elegans*. *Genomics*, **46**, 200–216.
41. Consortium, S. (1998) Genome sequence of the nematode *C. elegans*: a platform for investigating biology. *Science*, **282**, 2012–2018.
42. Ashrafi, K., Chang, F., Watts, J., Fraser, A., Kamath, R., Ahringer, J. *et al.* (2003) Genome-wide RNAi analysis of *Caenorhabditis elegans* fat regulatory genes. *Nature*, **421**, 268–272.
43. Hariharan, I.K. and Haber, D.A. (2003) Yeast, flies, worms, and fish in the study of human disease. *N. Engl. J. Med.*, **348**, 2457–2463.
44. Markaki, M. and Tavernarakis, N. (2010) Modeling human diseases in *Caenorhabditis elegans*. *Biotechnol. J.*, **5**, 1261–1276.
45. Chan, M.-S. (1997) The global burden of intestinal nematode infections—fifty years on. *Parasitol. Today*, **13**, 438–443.
46. Knox, D.P., Geldhof, P., Visser, A., and Britton, C. (2007) RNA interference in parasitic nematodes of animals: a

reality check? *Trends Parasitol.*, **23**, 105–107.
47. Lewis, J., Elmer, J., Skimming, J., McLafferty, S., Fleming, J., and McGee, T. (1987) Cholinergic receptor mutants of the nematode *Caenorhabditis elegans*. *J. Neurosci.*, **7**, 3059–3071.
48. Fleming, J., Squire, M., Barnes, T., Tornoe, C., Matsuda, K., Ahnn, J. *et al.* (1997) *Caenorhabditis elegans* levamisole resistance genes lev-1, unc-29, and unc-38 encode functional nicotinic acetylcholine receptor subunits. *J. Neurosci.*, **17**, 5843–5857.
49. Gally, C., Eimer, S., Richmond, J., and Bessereau, J. (2004) A transmembrane protein required for acetylcholine receptor clustering in *Caenorhabditis elegans*. *Nature*, **431**, 578–582.
50. Ellerbrock, B.R., Coscarelli, E.M., Gurney, M.E., and Geary, T.G. (2004) Screening for presenilin inhibitors using the free-living nematode, *Caenorhabditis elegans*. *J. Biomol. Screen.*, **9**, 147–152.
51. Pulak, R. (2006) Techniques for analysis, sorting, and dispensing of *C. elegans* on the COPAS™ flow-sorting system. *Methods Mol. Biol.*, **351**, 275–286.
52. Dupuy, D., Bertin, N., Hidalgo, C.A., Venkatesan, K., Tu, D., Lee, D. *et al.* (2007) Genome-scale analysis of in vivo spatiotemporal promoter activity in *Caenorhabditis elegans*. *Nat. Biotechnol.*, **25**, 663–668.
53. Doitsidou, M., Flames, N., Lee, A.C., Boyanov, A., and Hobert, O. (2008) Automated screening for mutants affecting dopaminergic-neuron specification in *C. elegans*. *Nat. Methods*, **5**, 869–872.
54. Squiban, B., Belougne, J., Ewbank, J., and Zugasti, O. (2012) Quantitative and automated high-throughput genome-wide RNAi screens in *C. elegans*. *J. Visualized Exp.*, **60**, 3448.
55. Stroustrup, N., Ulmschneider, B., Nash, Z., López-Moyado, I., Apfeld, J., and Fontana, W. (2013) The *Caenorhabditis elegans* lifespan machine. *Nat. Methods*, **10**, 665–670.
56. Whitesides, G.M., Ostuni, E., Takayama, S., Jiang, X., and Ingber, D.E. (2001) Soft lithography in biology and biochemistry. *Annu. Rev. Biomed. Eng.*, **3**, 335–373.
57. Daniel, J.H., Iqbal, S., Millington, R.B., Moore, D.F., Lowe, C.R., Leslie, D.L. *et al.* (1998) Silicon microchambers for DNA amplification. *Sens. Actuators, A*, **71**, 81–88.
58. Xia, Y. and Whitesides, G.M. (1998) Soft lithography. *Annu. Rev. Mater. Sci.*, **28**, 153–184.
59. Duffy, D.C., McDonald, J.C., Schueller, O.J., and Whitesides, G.M. (1998) Rapid prototyping of microfluidic systems in poly (dimethylsiloxane). *Anal. Chem.*, **70**, 4974–4984.
60. Whitesides, G.M. (2006) The origins and the future of microfluidics. *Nature*, **442**, 368–373.
61. Kirby, B. (2010) *Micro- and Nanoscale Fluid Mechanics*, vol. 32, Cambridge University Press, New York.
62. Nguyen, N.-T. and Wereley, S.T. (2002) *Fundamentals and Applications of Microfluidics*, Artech House.
63. Conant, C.G., Schwartz, M.A., Beecher, J.E., Rudoff, R.C., Ionescu-Zanetti, C., and Nevill, J.T. (2011) Well plate microfluidic system for investigation of dynamic platelet behavior under variable shear loads. *Biotechnol. Bioeng.*, **108**, 2978–2987.
64. Jang, J.S., Simon, V.A., Feddersen, R.M., Rakhshan, F., Schultz, D.A., Zschunke, M.A. *et al.* (2011) Quantitative miRNA expression analysis using fluidigm microfluidics dynamic arrays. *BMC Genomics*, **12**, 144.
65. Lee, J., Ghorashian, N., Gaige, T.A., and Hung, J. (2007) Microfluidic system for automated cell-based assays. *J. Assoc. Lab. Autom.*, **12**, 363–367.
66. Ghorashian, N., Gökçe, S.K., Guo, S.X., Everett, W.N., and Ben-Yakar, A. (2013) An automated microfluidic multiplexer for fast delivery of *C. elegans* populations from multiwells. *PLoS One*, **8**, e74480.
67. Hua, Z., Xia, Y., Srivannavit, O., Rouillard, J.-M., Zhou, X., Gao, X. *et al.* (2006) A versatile microreactor platform featuring a chemical-resistant

microvalve array for addressable multiplex syntheses and assays. *J. Micromech. Microeng.*, **16**, 1433.

68. Wang, J., Sui, G., Mocharla, V., Lin, R.J., Phelps, M.E., Kolb, H.C. *et al.* (2006) Integrated microfluidics for parallel screening of an in situ click chemistry library. *Angew. Chem.*, **118**, 5402–5407.
69. Gómez-Sjöberg, R., Leyrat, A.A., Pirone, D.M., Chen, C.S., and Quake, S.R. (2007) Versatile, fully automated, microfluidic cell culture system. *Anal. Chem.*, **79**, 8557–8563.
70. Singhal, A., Haynes, C.A., and Hansen, C.L. (2010) Microfluidic measurement of antibody – antigen binding kinetics from low-abundance samples and single cells. *Anal. Chem.*, **82**, 8671–8679.
71. Rohde, C.B., Zeng, F., Gonzalez-Rubio, R., Angel, M., and Yanik, M.F. (2007) Microfluidic system for on-chip high-throughput whole-animal sorting and screening at subcellular resolution. *Proc. Natl. Acad. Sci. U.S.A.*, **104**, 13891–13895.
72. Strange, K. (2006) *C. elegans: Methods and Applications*, vol. 351, Springer-Verlag.
73. Chokshi, T.V., Bazopoulou, D., and Chronis, N. (2010) An automated microfluidic platform for calcium imaging of chemosensory neurons in *Caenorhabditis elegans*. *Lab Chip*, **10**, 2758–2763.
74. Chronis, N., Zimmer, M., and Bargmann, C.I. (2007) Microfluidics for in vivo imaging of neuronal and behavioral activity in *Caenorhabditis elegans*. *Nat. Methods*, **4**, 727–731.
75. Chronis, N. (2010) Worm chips: microtools for *C. elegans* biology. *Lab Chip*, **10**, 432–437.
76. Qin, J. and Wheeler, A.R. (2007) Maze exploration and learning in *C. elegans*. *Lab Chip*, **7**, 186–192.
77. Hulme, S.E., Shevkoplyas, S.S., Apfeld, J., Fontana, W., and Whitesides, G.M. (2007) A microfabricated array of clamps for immobilizing and imaging *C. elegans*. *Lab Chip*, **7**, 1515–1523.
78. Kim, N., Dempsey, C.M., Zoval, J.V., Sze, J.-Y., and Madou, M.J. (2007) Automated microfluidic compact disc (CD) cultivation system of *Caenorhabditis elegans*. *Sens. Actuators, B*, **122**, 511–518.
79. Chung, K., Crane, M.M., and Lu, H. (2008) Automated on-chip rapid microscopy, phenotyping and sorting of *C. elegans*. *Nat. Methods*, **5**, 637–643.
80. Zeng, F., Rohde, C.B., and Yanik, M.F. (2008) Sub-cellular precision on-chip small-animal immobilization, multi-photon imaging and femtosecond-laser manipulation. *Lab Chip*, **8**, 653–656.
81. Guo, S.X., Bourgeois, F., Chokshi, T., Durr, N.J., Hilliard, M.A., Chronis, N. *et al.* (2008) Femtosecond laser nanoaxotomy lab-on-a-chip for in vivo nerve regeneration studies. *Nat. Methods*, **5**, 531–533.
82. Lockery, S.R., Lawton, K.J., Doll, J.C., Faumont, S., Coulthard, S.M., Thiele, T.R. *et al.* (2008) Artificial dirt: microfluidic substrates for nematode neurobiology and behavior. *J. Neurophysiol.*, **99**, 3136–3143.
83. Lockery, S.R., Hulme, S.E., Roberts, W.M., Robinson, K.J., Laromaine, A., Lindsay, T.H. *et al.* (2012) A microfluidic device for whole-animal drug screening using electrophysiological measures in the nematode *C. elegans*. *Lab Chip*, **12**, 2211–2220.
84. Chung, K. and Lu, H. (2009) Automated high-throughput cell microsurgery on-chip. *Lab Chip*, **9**, 2764–2766.
85. Gilleland, C.L., Rohde, C.B., Zeng, F., and Yanik, M.F. (2010) Microfluidic immobilization of physiologically active *Caenorhabditis elegans*. *Nat. Protoc.*, **5**, 1888–1902.
86. Rezai, , Siddiqui, A., Selvaganapathy, R., and Gupta, B. (2010) Electrotaxis of *Caenorhabditis elegans* in a microfluidic environment. *Lab Chip*, **10**, 220–226.
87. Rezai, P., Siddiqui, A., Selvaganapathy, P.R., and Gupta, B.P. (2010) Behavior of *Caenorhabditis elegans* in alternating electric field and its application to their localization and control. *Appl. Phys. Lett.*, **96**, 153702-1–153702-3.
88. Hulme, S.E., Shevkoplyas, S.S., McGuigan, A., Apfeld, J., Fontana, W.,

and Whitesides, G.M. (2010) Lifespan-on-a-chip: microfluidic chambers for performing lifelong observation of *C. elegans*. *Lab Chip*, **10**, 589–597.

89. Shi, W., Wen, H., Lu, Y., Shi, Y., Lin, B., and Qin, J. (2010) Droplet microfluidics for characterizing the neurotoxin-induced responses in individual *Caenorhabditis elegans*. *Lab Chip*, **10**, 2855–2863.
90. Albrecht, D.R. and Bargmann, C.I. (2011) High-content behavioral analysis of *Caenorhabditis elegans* in precise spatiotemporal chemical environments. *Nat. Methods*, **8**, 599–605.
91. Crane, M.M., Stirman, J.N., Ou, C.-Y., Kurshan, T., Rehg, J.M., Shen, K., and Lu, H. (2012) Autonomous screening of *C. elegans* identifies genes implicated in synaptogenesis. *Nat. Methods*, **9**, 977–980.
92. Ding, X., Lin, S.-C.S., Kiraly, B., Yue, H., Li, S., Chiang, I.-K. *et al.* (2012) On-chip manipulation of single microparticles, cells, and organisms using surface acoustic waves. *Proc. Natl. Acad. Sci. U.S.A.*, **109**, 11105–11109.
93. Wang, X., Tang, L., Xia, Y., Hu, L., Feng, X., Du, W. *et al.* (2013) Stress response of *Caenorhabditis elegans* induced by space crowding in a micro-column array chip. *Integr. Biol.*, **5**, 728–737.
94. Larsch, J., Ventimiglia, D., Bargmann, C.I., and Albrecht, D.R. (2013) High-throughput imaging of neuronal activity in *Caenorhabditis elegans*. *Proc. Natl. Acad. Sci. U.S.A.*, **110**, 4266–4273.
95. Hu, C., Dillon, J., Kearn, J., Murray, C., O'Connor, V., Holden-Dye, L. *et al.* (2013) NeuroChip: a microfluidic electrophysiological device for genetic and chemical biology screening of *Caenorhabditis elegans* adult and larvae. *PLoS One*, **8**, e64297.
96. Johari, S., Nock, V., Alkaisi, M.M., and Wang, W. (2013) On-chip analysis of *C. elegans* muscular forces and locomotion patterns in microstructured environments. *Lab Chip*, **13**, 1699–1707.
97. Kopito, R.B. and Levine, E. (2014) Durable spatiotemporal surveillance of *Caenorhabditis elegans* response to environmental cues. *Lab Chip*, **14**, 764–770.
98. Allen, B., Sgro, A.E., Chao, D.L., Doepker, B.E., Scott Edgar, J., Shen, K. *et al.* (2008) Single-synapse ablation and long-term imaging in live *C. elegans*. *J. Neurosci. Methods*, **173**, 20–26.
99. Ben-Yakar, A., Chronis, N., and Lu, H. (2009) Microfluidics for the analysis of behavior, nerve regeneration, and neural cell biology in *C. elegans*. *Curr. Opin. Neurobiol.*, **19**, 561–567.
100. Chuang, H.-S., Raizen, D.M., Lamb, A., Dabbish, N., and Bau, H.H. (2011) Dielectrophoresis of *Caenorhabditis elegans*. *Lab Chip*, **11**, 599–604.
101. Chung, K., Zhan, M., Srinivasan, J., Sternberg, W., Gong, E., Schroeder, F.C. *et al.* (2011) Microfluidic chamber arrays for whole-organism behavior-based chemical screening. *Lab Chip*, **11**, 3689–3697.
102. Stirman, J.N., Brauner, M., Gottschalk, A., and Lu, H. (2010) High-throughput study of synaptic transmission at the neuromuscular junction enabled by optogenetics and microfluidics. *J. Neurosci. Methods*, **191**, 90–93.
103. Vidal-Gadea, A., Ward, K., Beron, C., Ghorashian, N., Gokce, S., Russell, J. *et al.* (2015) Magnetosensitive neurons mediate geomagnetic orientation in *Caenorhabditis elegans*. *Elife*, **4**, doi: 10.7554/eLife.07493.
104. Chokshi, T., Ben-Yakar, A., and Chronis, N. (2009) CO_2 and compressive immobilization of *C. elegans* on-chip. *Lab Chip*, **9**, 151–157.